https://doi.org/10.5194/amt-2023-113
Preprint. Discussion started: 24 July 2023

Atmospheric Measurement Techniques Discussions

Application of a new UAV measurement methodology to the quantification of CO_2 and CH_4 emissions from a major coking plant

Tianran Han[1], Conghui Xie[1], Yayong Liu[1], Yanrong Yang[1], Yuheng Zhang[1], Yufei Huang[1], Xiangyu Gao[2], Xiaohua Zhang[3], Fangmin Bao[4], Shao-Meng Li[1]

[1] State Key Joint Laboratory of Environmental Simulation and Pollution Control, College of Environmental Sciences and Engineering, Peking University, Beijing 100871, P.R. China
[2] Beijing Wisdominc Technology Co., Ltd., Beijing, P.R. China
[3] Suzhou Environmental Monitoring Center, Jiangsu Province, P.R. China
[4] Jiangsu Shagang Group Co., Ltd., Beijing, P.R. China

Correspondence to: Shao-Meng Li (shaomeng.li@pku.edu.cn)

Abstract. The development in unmanned aerial vehicle (UAV) technologies over the past decade has led to a plethora of platforms that can potentially enable greenhouse gas measurements over the 3-dimensional space. Here, we report the development of a new air sampler, consisting of a pumped stainless tube of 150 m in length with controlled time-stamping, and its deployment from an industrial UAV to quantify CO_2 and CH_4 emissions from the main coking plant stacks of a major steel maker in eastern China. During flights, the air sampler starts sampling as soon as the UAV takes off, and stops sampling after landing. The air sample is immediately analyzed upon retrieval with a CRDS gas analyzer for CO_2 and CH_4 mixing ratios. Laboratory tests show that the time series of CO_2 and CH_4 measured using the sampling system is smoothed when compared to online measurement by the CRDS analyzer. Further analyses show that the smoothing is akin to a convolution of the true time series signals with a heavy-tailed digital filter. For field test, the air sampler was mounted on the UAV and flown virtual boxes around two stacks in the coking plant at Shagang Steel Group. Mole fractions of CO_2 and CH_4 in air and meteorological parameters were measured from the UAV during the test flight. A mass-balance computational algorithm was used on the data to estimate the CO_2 and CH_4 emission rates from the stacks. Using this algorithm, the emission rates for the two stacks from the coking plant were calculated to be 0.12±0.014 t h^{-1} for CH_4 and 110±18 t h^{-1} for CO_2, the latter being in excellent agreement with material balance based estimates. A Gaussian plume inversion approach was also used to derive the emission rates and the results were compared with those derived using the mass-balance algorithm, showing a good agreement between the two methods.

https://doi.org/10.5194/amt-2023-113
Preprint. Discussion started: 24 July 2023

1 Introdution

Atmospheric carbon dioxide (CO_2) and methane (CH_4) are the two major anthropogenic greenhouse gases (GHGs). Both CO_2 and CH_4 in the atmosphere have been increasing since the industrial revolution, particularly rapidly over the past ten years. Global networks consistently show that the globally averaged annual mean CO_2 molar fraction in the atmosphere increased by 5.0% from 2011 to 2019, reaching 409.9 ± 0.4 ppm in 2019. Likewise, the globally averaged surface atmospheric molar fraction of CH_4 in 2019 was 1866.3 ± 3.3 ppb, 3.5% higher than in 2011(Gulev, 2021). CH_4 is a stronger absorber of Earth's thermal infrared radiation than CO_2, with its global warming potential (GWP) 32 times greater than that of CO_2 over a 100-year horizon(Saunois et al., 2020). Although its molar fractions in the atmosphere are about 200 times lower than those of CO_2, the total radiative forcing of ~1.0 W m^{-2} for CH_4 is about half of that of CO_2 (~2 W m^{-2})(Arias, 2021) , contributed by its direct radiative forcing of (0.6±0.1) W m^{-2} and indirect forcing of 0.4 W m^{-2} resulting from chemical reactions producing other GHGs including CO_2, O_3, and stratospheric water(Turner et al., 2019). Furthermore, although global anthropogenic CH_4 emissions are estimated to be only 3% of the global anthropogenic CO_2 emissions in units of carbon mass flux, the increase in atmospheric CH_4 is responsible for about 20% of the warming induced by long-lived greenhouse gases since pre-industrial times(Etminan et al., 2016). Both CO_2 and CH_4 are produced and released into the atmosphere from a variety of natural and anthropogenic sources. Natural emission sources include vegetation, oceans, volcanoes and naturally occurring wildfires, but most of the increases in atmospheric CO_2 and CH_4 are considered to have resulted from anthropogenic emissions, from sources including fossil fuel production and uses, agricultural activities, land use and industrial processes(Canadell, 2021).

Quantification of CO_2 and CH_4 emissions from sources requires continuous measurements of their mole fractions as well as meteorological parameters using a variety of stationary and mobile platforms, including ground-based vehicles(Rella et al., 2015; Brantley et al., 2014), towers(Helfter et al., 2016; Takano and Ueyama, 2021), aircrafts(Li et al., 2017; Liggio et al., 2019) and sattellites(Miller et al., 2013; Turner et al., 2015). Small unmanned aerial vehicles (UAVs) have become emerging platforms due to the recent rapid technological developments. They are flexible, versatile and relatively inexpensive. Most importantly, a UAV platform could fill the sampling space between the ground, and altitudes of up to hundreds of meters above ground, in which other mobile platforms have been unable to operate(Shaw et al., 2021). Due to their relatively low flying speeds, UAV platforms could offer a high spatiotemporal resolution for sampling and thus enabling accurate plume mapping. On the other hand, UAVs have limited endurance, being constrained by battery capacities and payloads, making them more suitable for small facility flux quantification.

https://doi.org/10.5194/amt-2023-113
Preprint. Discussion started: 24 July 2023

UAV platforms have been used to quantify CH_4 emissions in several studies, mainly focused on facility-scale emission sources including landfills(Allen et al., 2019; Bel Hadj Ali et al., 2020), coal mines(Andersen et al., 2021), dairy farms(Vinkovic et al., 2022), wastewater treatment plants(Galfalk et al., 2021) and oil and gas facilities(Golston et al., 2018; Li et al., 2020; Nathan et al., 2015; Shah et al., 2020; Tuzson et al., 2021). UAV-based CH_4 measurements are generally made with three different methods: collecting on-board samples for subsequent analysis, tethered sampling to a sensor on the ground and on-line measurements(Shaw et al., 2021). Gas samples could be stored onboard a UAV for subsequent analyses on the ground after landing, using air bags(Brownlow et al., 2016) or sampling canisters(Chang et al., 2016). Anderson et al.(2018) developed a UAV-based active aircore system, consisting of a long coiled stainless-steel tubing, a small pinhole orifice, and a pump that drags air through the tube(Andersen et al., 2018), which allows for a higher spatiotemporal resolution in the measurements. Direct comparisons between a quantum cascade laser absorption spectrometer (QCLAS) and the active aircore measurements show that the active aircore measurements are smoothed by 20 s and had an average time lag of 7 s. The active aircore measurements also stretch linearly with time at an average rate of 0.06 s for every second of QCLAS measurement(Morales et al., 2022). The advances in active aircore sampling have made UAV measurements for CH_4 emissions feasible, even if still with rooms for improvement. To the best of our knowledge, there have been no reports of using UAVs to determine CO_2 emission rates from anthropogenic sources.

In this study, we developed a new active air sampling system for deployment from a UAV for three-dimensional measurements of CO_2 and CH_4. The complete sampler plus UAV system was deployed to quantify CO_2 and CH_4 emissions from the stacks of the main coking plant of Shagang, the largest private steel maker in China. The top-down emission rate retrieval algorithm (TERRA)(Gordon et al., 2015) was applied to the UAV data to determine stack CH_4 and CO_2 emissions rates. The iron and steel industry is one of the largest contributing industries to global GHG emissions, accounting for around 7% of global total GHG emissions(Hasanbeigi, 2022). Coke production is one major process of iron and steel making that generate emissions of CO_2 and CH_4. During coke production, coking coal is used to manufacture metallurgical coke that is subsequently used as the reducing agent in the production of iron and steel(U.S. Environmental Protection Agency, 2016). Coke oven gas is the main sources of CO_2 and CH_4 emissions during coke production(Angeli et al., 2021; IPCC, 2006). China is the largest coke producer in the world, with a coke production of 4.72 billion tons in 2020(CEIC, 2021) . The GHG emissions from coke production in China are reported based on the Tier 1 methodology of IPCC Guidelines, which multiplies generic default emission factors with the tonnage of coke produced(Ministry of Ecology and Environment of of China, 2018). The present UAV measurement-based emission results can be compared with material balance based emission estimates and the emissions based on the Tier 1 emission factors and coke

https://doi.org/10.5194/amt-2023-113
Preprint. Discussion started: 24 July 2023

Atmospheric Measurement Techniques Discussions

production at the plant, and to shed light on the uncertainties related to Tier 1 emission factors in the case of CH_4 emissions.

2.Method

2.1 The air sampling system

To realize GHG emission quantification by UAV measurement, a new compact air sampling system was developed based on a variation of the active aircore method(Karion et al., 2010). Figure 1 shows an overview of the patent-pending design for this sampler. It consists of a 150 m long thin-walled 1/8 inch outside diameter stainless-steel tubing, a pump, a micro-orifice, a CO_2 marker generator, two three-way solenoid valves and electric relays, with all electrical devices powered by a 12V battery. The tubing is winded into a multilayer coil, in whose center the other components of the system are mounted. The system is housed in the highly compact patent-pending carbon fiber assembly design of 280 mm diameter and 98 mm height, that can be quickly mounted at and dismounted from the bottom of an UAV. The sampler weighs about 5.9 kg and allows for continuous sampling up to 35 minutes.

The sampler air intake is mounted at 45 cm above the center of gravity of the UAV, placed nearby a sonic anemometer (below) for ensuring sampling the same air mass where wind speed is measured. The time stamp of the mole fraction observation was corrected for the short time lag of 4 seconds between sampling at the air intake and the thin-walled stainless-steel tubing attributable to the length of the Teflon inlet tube. Shortly before every flight, the pump is remotely turned on to sample the CO_2 marker for 5 seconds to mark the beginning of the flight, and then to collect air samples. During flight, the pump would alternatively sample the marker and the ambient air on a preset timing schedule. The sampling flow rate remains at 18 ccm during the entire flight, controlled with the micro-orifice which is placed between the pump and the coiled tubing. After landing, the pump is remotely turned off and the air sample in the sampling tubing is immediately analyzed with a cavity ring down spectrometer (CRDS) (Picarro, Inc., CA, USA, model G2401) for CO_2 and CH_4 mixing ratios in the sampled air. Using the embedded CO_2 marker data, the CO_2 and CH_4 data series can be mapped to the sampling times and GPS locations during flight.

https://doi.org/10.5194/amt-2023-113
Preprint. Discussion started: 24 July 2023

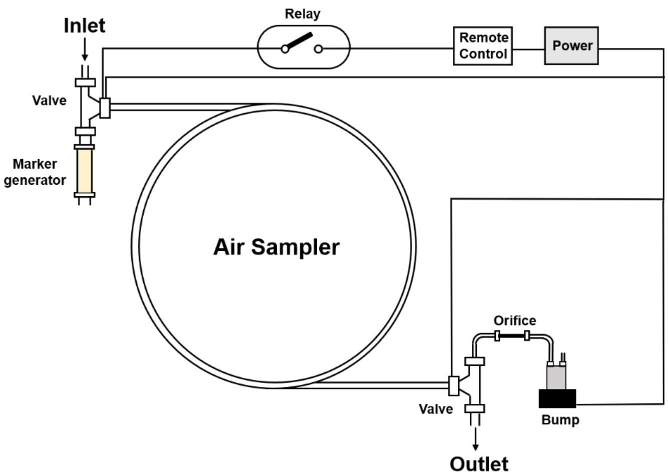

Figure 1. Design of the air sampler

2.2 The 3D sonic anemometer

Previous studies that applied UAV platforms for GHG monitoring generally relied wind data from nearby ground weather stations(Morales et al., 2022; Allen et al., 2019). However, Gålfalk et al.(2021) shows that wind speeds were inconsistent between a ground weather station at a 1.5 m height and an anemometer mounted on their UAV, especially when altitude increases, showing the need to have an on-board weather station for accurate flux calculations(Galfalk et al., 2021). In the present study, in order to obtain meteorological data along the flight track, a 3D sonic anemometer (Geotech Inc, Denver, US, model Trisonica Mini) is attached on the top of the UAV via a 450 mm carbon fiber pole. The anemometer measures wind speeds within the range of 0-50 m s^{-1}, with an accuracy of ±0.1 m s^{-1} below the wind speed of 10 m/s. The accuracy for wind direction measurement is ±1°. For temperature measurement, the operating range for the anemometer is between -40°C to 85°C and the accuracy is ±2°C.

For anemometers mounted on multi-rotor UAVs, how to correct for the effects of the translational and rotational movements of the UAVs as well as the flows induced by the rotors to obtain accurate wind data is an on-going research topic(Galfalk et al., 2021; Wolf et al., 2017; De Boisblanc et al., 2014; Palomaki et al., 2017; Zhou et al., 2018; Yang, 2023). During flight, rotary wing UAVs create thrust by drawing air from above the rotors and expelling it downwards at a higher velocity. Such flows may extend to the anemometer position in addition to true atmospheric air flows, masking the true wind signals in the data from the anemometer(Wolf et al., 2017). Previous studies have conducted laboratory testing(Wolf et al., 2017; De Boisblanc et al., 2014; Palomaki et al., 2017) or flow field simulation(Zhou et al., 2018) to

https://doi.org/10.5194/amt-2023-113
Preprint. Discussion started: 24 July 2023

determine the appropriate distance to place anemometers onto multi-rotor UAVs to minimize the impact from the rotor-induced air flows. The anemometer in this research is mounted at an upward distance of 45 cm from the center of gravity of the UAV to minimize this interference based on the results from flow field simulations for combinations of the UAV flight envelope and true winds, and verified with UAV flight-meteorological tower measurement intercomparisons(Yang, 2023). During the flight, the meteorological data including wind speed, wind direction and temperature were transmitted and collected on ground. The data are post-flight corrected for the rotor-induced air flows, the true air speeds of the UAV, and the UAV attitude changes during flight to derive accurate wind speed and direction results(Yang, 2023) along the flight track.

2.3 The UAV

The air sampler and the anemometer are mounted on a hexacopter UAV (KWT-X6L-15). The UAV has a maximum flight time of ~30 minutes at a maximum payload of 15 kg, or longer with a lighter payload. Such flight endurance and carrying capacity meet our needs for loading the air sampler and the anemometer onto the UAV to realize emission quantification. The UAV is capable of flying at winds up to 14.4 m s^{-1} to an altitude of about 4000 m and has a maximum horizontal flying speed of 18 m s^{-1}, a maximum ascending speed of 4 m s^{-1} and a maximum descending speed of 3m s^{-1}. The horizontal precision of the GPS on the UAV is ± 2 m and the vertical precision is ±1.5 m.

2.4 Air sample analysis

After landing, the air sample collected in the tubing is immediately analyzed with the CRDS analyzer. The withdrawal flow rate of the air from the sample tubing during analysis is an important parameter in optimizing the results; high withdrawal rates lead to unwanted mixing in the cavity of the analyzer. However, direct withdrawal of air from the sample tubing by the analyzer at a flow rate as low as the sampling flow rate of 18 sccm results in smoothing of concentrations from the laminar flow inside the tubing. We optimized the flow rate of the air from the sample tubing into the CRDS analyzer at ~ 54 sccm, 3 times the sampling flow rate, by diluting the air sample with zero air, with two mass flow controllers separately controlling the flow rate of zero air and the withdrawal rate of the air sample.

3 Validation of the air sampler: laboratory tests

Prior to flights in the field, we validated the air sampler in laboratory experiments by sampling a mixture of lab air/standards of CO_2, CH_4 and comparing the results from the air sampling/CRDS analysis with those from simultaneous online measurement of the same lab air mixture with the CRDS analyzer. An experimental apparatus was constructed for

https://doi.org/10.5194/amt-2023-113
Preprint. Discussion started: 24 July 2023

Atmospheric Measurement Techniques
Discussions

simultaneous sampling of the same lab air mixture with the air sampler and the online measurement through a tee junction (Fig. 2(a)) and subsequent air sample analysis using the same analyzer (Fig. 2(b)). The CH_4 and CO_2 standards were control-released into the lab air from an 8 L gas cylinder filled with a gas mixture of 5 ppm CH_4, 2 ppm CO and 600 ppm CO_2. The outlet of the standard gas cylinder was held at artificially different distances to the tee junction over time to yield a time series of different CH_4 and CO_2 mixing ratios in the mixed lab air/standards, which was designed to mimic plumes expected in the real atmosphere. During analysis, the flow rate through MFC 1 is adjusted to make sure that the flow rate through MFC 2 is stable and consistent at 54 sccm (Section 2.4).

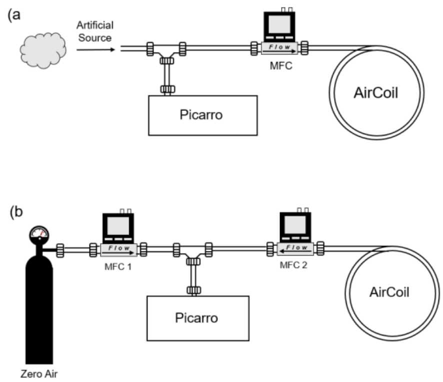

Figure 2. Diagram of the new air sample system testing setup in the laboratory. (a) simultaneous sampling by the air sampler and the Picarro CRDS analyzer. (b) subsequent air sample analysis using the analyzer.

Figure 3 (a) illustrates the mole fractions of CO_2 and CH_4 measured by the air sampler followed by the CRDS analysis. It can be seen that the measured samples and the online measurements are in good agreement throughout the tests. For the measurements with the air sampler, short term variations and noises, that were fully captured by the online measurement, were smoothed out, while the main features and tendency were preserved. In fact, the air sampler measurement result should be a smoothed version of the online measurement, due to mixing in the analyzer cavity, molecular diffusion during sample storage in the sampler, inner wall surface drag and desorption during its withdrawal from the tubing during analysis, as well as Taylor dispersion during sampling and analysis(Karion et al., 2010). Dilution with zero air during CRDS analysis also contributes to the smoothing.

4. Data deconvolution to achieve high time resolution

While it is impractical to delineate the individual smoothing effects when the air sample passes through the coupled system of the sampler plus the analysis setup as described above, the measured concentration $y(t)$ can be treated as a

https://doi.org/10.5194/amt-2023-113
Preprint. Discussion started: 24 July 2023

Atmospheric Measurement Techniques Discussions
Open Access
EGU

result of the convolution of the air concentration before sampling $x(t)$ and a smoothing kernel $g(i)$ consisting of a series of weights, which are inherently determined by factors including the sampler properties (tubing length, inner diameter, temperature, absorptive properties, flow rates), storage time, dilution, and mixing in the cavity of the instrument. The smoothing can be described as

$$y(t) = \sum_{i=r}^{s} g(i)x(t-i) + n(t), t = s, s+1, \dots, n-1+r \quad (1)$$

Or, expressed as a convolution of the form

$$y(t) = g(t) * x(t) + n(t) \quad (2a)$$

where $y(t)$ is the measured concentration at time t, $x(t)$ the air concentration, and $n(t)$ the unknown noise, assumed to be independent of $x(t)$. The kernel $g(i)$ contains $s-r+1$ non-zero kernel weight terms ($0 < g(i) < 1$). When all four terms in Eq. (2a) undergo Fourier transform, Eq. (2a) can be expressed in the frequency domain

$$Y(f) = G(f)X(f) + N(f) \quad (2b)$$

In order to characterize the kernel weights $g(i)$, a second lab experiment was conducted during which the sampler first sampled zero air for some time, and then sampled the CO_2 and CH_4 standards for one second, before returning to sampling zero air again, creating an original concentration pulse signal in the $x(t)$:

$$x(t) = \begin{cases} C, & t = j \\ 0, & t \neq j \end{cases} \quad (3)$$

where $j = j^{th}$ second when the sampler collected the standard of a known concentration C. This air sample was then analyzed with the CRDS as described above. After sampling, storing and analyzing, smoothing of the original concentration pulse leads to the concentration signal output $Y(t)$ as follows:

$$y(t) = \begin{cases} \sum_{i=r}^{s} g(i)x(t-i) + n(t) = g(t-j)C + n(t), & t-i = j \; and \; i = r, r+1, \cdots, s \\ n(t), & t-i \neq j \end{cases} \quad (4)$$

where $y(t)$ is the measured concentrations from the air sampler after sampling the concentration pulse and is non-zero when $t-i=j$, with the index i taking the values from r to s. The noise $n(t)$ term is zero for $t-i \neq j$ and can be assumed to have similar behavior for $t-i=j$. Therefore,

$$g(i) = g(t-j) = \frac{1}{C}y(t) - \frac{1}{C}n(t), \; t = i+j \; and \; i = r, r+1, \cdots, s \quad (5)$$

The second lab experiment showed that $y(t)$, and therefore the kernel $g(t)$, consists of 70 non-zero values. To remove the noise $n(t)$, $g(t)$ is further smoothed using a box-car running mean of 5 terms

$$\hat{g}(t) = \frac{1}{5}\sum_{k=t-2}^{k=t+2} g(k) \approx \frac{1}{C}y(t), \; t = i+j \; and \; i = r, r+1, \cdots, s \quad (6)$$

It could be seen from Fig. 3(b) that $\hat{g}(t)$ has an asymmetrical distribution with a right trailing tail and a half-height width of approximately 20 seconds for CO_2 and 21 seconds for CH_4, indicating that the smoothing had significantly reduced the

https://doi.org/10.5194/amt-2023-113
Preprint. Discussion started: 24 July 2023

Atmospheric Measurement Techniques
Open Access
Discussions

sampling/analysis method time resolution to about 20 second from the 1 second resolution of the original pulse in the air concentration. The kernel shows that the influence from the neighboring points have on a given point decreases with increases in the gap between the two points.

To test whether the kernel weights $\hat{g}(t)$ can smooth the online measured concentrations from the first lab experiment (top data series in Fig. 3(a), left), the weights $\hat{g}(t)$ were used to convolute with the data from the online measurements (i.e., $x(t)$), resulting in an estimated $\hat{y}(t)$ (Fig. 3(a), third curve) that is in excellent agreement with the measurements from the sampler/analysis process (the second curve in Fig. 3(a)).

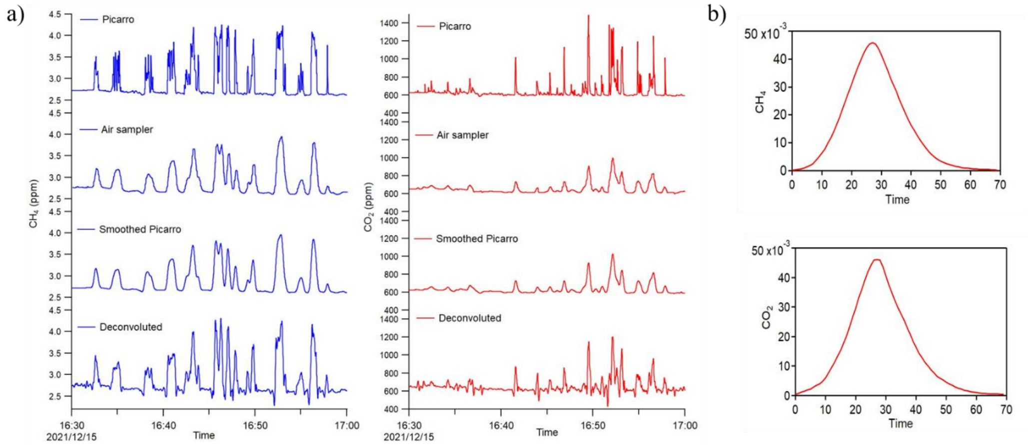

Figure 3.(a) Mole fraction of CO_2 and CH_4 measurements by online measurements with CRDS (first) and sampling/analysis (second) in laboratory tests. The third line represents the smoothed CRDS data after convolution with the kernel $\hat{g}(t)$ and the fourth line represents the deconvoluted series after Wiener deconvolution. (b) The output of the one-second signal after sampling, storing and analyzing using the air sampler for CO_2 and CH_4, normalized by their respective concentrations in the standard. As shown in the text, these curves are the actual kernel weights of $\hat{g}(t)$.

The ultimate goal of determining $\hat{g}(t)$ in Fig. 3(b) is to deconvolve $y(t)$ from the sampling/analysis process to obtain the original concentration series $x(t)$ using a number of deconvolution techniques. In the present study, we used the deconvolution method based on the Wiener theorem(Lin and Jin, 2013). The theorem provides the Wiener convolution filter $h(t)$ so that $x(t)$ can be estimated as follows:

$$\hat{x}(t) = \sum_{i=-\infty}^{\infty} h(i)y(t-i) = h(t) * y(t) \tag{7}$$

where $y(t)$ is the measured concentration, and $\hat{x}(t)$ an estimate of $x(t)$. In the frequency domain, Eq. (7) may be rewritten as a product of two scalars:

$$\hat{X}(f) = H(f)Y(f) \tag{8}$$

https://doi.org/10.5194/amt-2023-113
Preprint. Discussion started: 24 July 2023

where $\hat{X}(f)$, $H(f)$, and $Y(f)$ are the Fourier transforms of $\hat{x}(t)$, $h(t)$, and $y(t)$, respectively.

The Wiener convolution filter $h(t)$ is derived from the minimization of the mean square error:

$$\epsilon(f) = E\left|X(f) - \hat{X}(f)\right|^2 \quad (9)$$

with E denoting the expectation. When Eq. (2b) and Eq. (8) are substituted into Eq. (9) and the quadratic is expanded, the mean square error $\epsilon(f)$ can be differentiated with respect to $H(f)$ and the derivative $\frac{d\epsilon(f)}{dH(f)}$ is set to zero to achieve the minimization; under the assumption that the noise $N(f)$ is independent of $X(f)$, $H(f)$ is derived as

$$H(f) = \frac{G(f)S(f)}{|G(f)|^2 S(f) + N(f)} \quad (10)$$

where $G(f)$ is the Fourier transform of $\hat{g}(t)$ derived from the second lab experiment described above, $S(f) = E|X(f)|^2$ and $N(f) = E|N(f)|^2$ are the mean power spectral densities of the original concentration series $x(t)$ and the noise $n(t)$, respectively. Equation (10) could be rewritten as:

$$H(f) = \frac{1}{G(f)}\left[\frac{|G(f)|^2}{|G(f)|^2 + N(f)/S(f)}\right] = \frac{1}{G(f)}\left[\frac{|G(f)|^2}{|G(f)|^2 + 1/SNR(f)}\right] \quad (11)$$

where $SNR(f) = S(f)/N(f)$ is the signal-to-noise ratio.

Substituting Eq. (11) into Eq. (8), $\hat{X}(f)$, the Fourier transforms of $\hat{x}(t)$, is derived. The deconvolution is completed with the inverse Fourier transform of $\hat{X}(f)$ to give $\hat{x}(t)$, the estimated air concentrations. The deconvolved series of CO_2 and CH_4 restored with the Wiener convolution filter are shown in Fig. 3(a), indicating the effectiveness of the Wiener theorem to deconvolve a smoothed series to a much higher time resolution while accounting for noise. The restored series is improved in terms of time resolution, from about 20 seconds mentioned above to about 3~4 seconds after the deconvolution. The lab test data from the online measurements contain strong high-frequency components, artificially manipulated to provide an extreme case for testing the deconvolution algorithm. Such high frequencies lead to some residual noise in the deconvolved results, primarily as a result of choosing the cutoff frequencies for the mean power spectral densities $S(f)$ and $N(f)$. Nevertheless, such a situation will be improved for sampling in the real atmosphere where sub-second high-frequency variations are not common.

5. Field application

To apply the UAV-based measurement system described above to atmospheric measurements of CO_2 and CH_4, flights were made at the Shagang Group located in Jiangsu, China on 28 December 2021. Shagang Group is a major iron and

https://doi.org/10.5194/amt-2023-113
Preprint. Discussion started: 24 July 2023

steel company on the south shore of the Yangtze River (31.9704° N, 120.6443° E). The company produces over 40 million tons of steel each year, making it one of China's top-five steel producers. Onsite coke making for iron production is located in the western part of the Shagang Steel complex. The coke making process is to dry distill coal in a coking oven at ~1000°C temperature to boil off volatile components to form coke (metallic coal). During coke production, combustion of coking oven gas, blast furnace gas from steel making, and coal tar plus light oil for heating the coking oven is the main CO_2 and CH_4 emission source.

Two coking plant stacks were chosen as the target emission source for the field UAV flight. During flight, the UAV was flown in a rectangle pattern (200m×500m) that encloses the two stacks, with repeated flight tracks at 9 altitude levels that, when stacked, created a virtual box and intercepted the emitted CO_2 and CH_4 plumes on the downwind side of the box. The UAV ascended from 15 m a.s.l. to 150 m a.s.l. and started the box flight at this altitude, ascending 15 m every level and reaching a maximum altitude of 270 m a.s.l. before landing. The UAV maintained a constant horizontal speed of 8 m s^{-1} during flight. After landing, the air sample collected in the sampler was immediately analyzed with the CRDS analyzer as per the procedure described above in Fig. 2.

CH_4 and CO_2 emission rates from both stacks were determined using a modified version of the Top-down Emission Rate Retrieval Algorithm (TERRA)(Gordon et al., 2015) using their measured mixing ratios and the meteorological data collected on board the UAV during the flight. TERRA is a mass balance algorithm, where pollutant emission rates are estimated based on the divergence theorem which equates the change in mass within a control volume with the integrated mass flux through the walls of the control volume plus the emission rates. It has been used successfully and extensively for emission rate determination of tens of volatile organic compounds(Li et al., 2017), CO_2(Liggio et al., 2019), CH_4(Baray et al., 2018), oxidized sulphur and nitrogen(Hayden et al., 2021), black carbon(Cheng et al., 2020), and secondary organic aerosol(Liggio et al., 2016) using aircraft measurements. In this study, the original TERRA is further modified and tailored to make use of the high resolution UAV-based measurements.

6. Result and discussion

6.1 CH_4 and CO2 mixing ratio enhancement from the coking plant

Figure 4(a) shows the time series of CH_4 and CO_2 mole fractions measured with the air sampler at the coking plant during the flight (red line). The air sampler sampled for a total of 30 minutes during the flight. After landing, the air sample was analyzed for 10 minutes, as the analysis flow rate triples the sampling flow rate (54.0 sccm vs. 18.0 sccm). The time scales

https://doi.org/10.5194/amt-2023-113
Preprint. Discussion started: 24 July 2023

of instrument readings were then stretched three times to restore the original time scales. The CH_4 and CO_2 time series were then deconvolved using the convolution kernel obtained from laboratory test (Section 3) to restore the mixing ratio time series in air (black line). The meteorological parameters during the time of flight were measured by the 3D anemometer, showing consistent southwesterly winds with a mean wind speed of 3.0 m s^{-1} (Fig. 5(b)). Consistency of wind measurements can be seen from the two wind rose plots for the northern wall and the southern wall respectively. During the flight, the maximum mixing ratio measured was 5.6 ppm for CH_4 and 1356 ppm for CO_2. During the 30-minute flight, a total of 5 CO_2 makers were generated during the 30 minutes of sampling (Fig. 5(a)), and the decreases in the marker concentrations are corrected with a Gaussian form function.

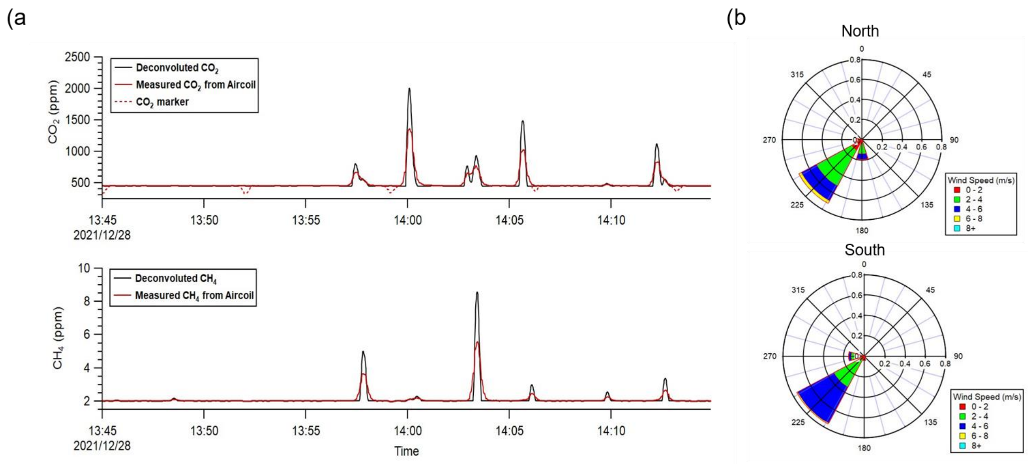

Figure 4.(a) Red line represents CH_4 and CO_2 mole fractions measured from the air samples collected with the air sampler during the flight in the coking plant. Black line represents the deconvolved CH_4 and CO_2 time series red dashed line sections represent the original marker CO_2 concentrations every 7 minutes. (b)Wind rose plot for the northern and southern wall based on the onboard meteorological measurements during the flight.

6.2 Emission estimation

The CO_2 and CH_4 emission rates for the stacks from coking plant were estimated by applying a version of the computation algorithm TERRA specifically modified to suit UAV measurements. The deconvolved mixing ratio time series of CO_2 and CH_4 were used in the TERRA algorithm. The algorithm first maps the mixing ratios to the walls of the virtual box, then applies a kriging scheme to interpolate the data and produces a 2 m (vertical) by 1 m (horizontal) mesh on the virtual box walls (200m×500m) (Fig. 5). Wind speed and wind direction are first decomposed into northly and easterly components, then further converted to vectors that are normal to and parallel to the walls of the virtual box before kriging. As shown in Fig. 5, the CH_4 and CO_2 plumes can be seen at different locations on the downwind side of the box wall,

https://doi.org/10.5194/amt-2023-113
Preprint. Discussion started: 24 July 2023

Atmospheric Measurement Techniques
Discussions

which indicates that the CH_4 plume and the CO_2 plume probably came from different sources within the box. Using the modified version of TERRA, the emission rates for the two stacks in the coking plant were calculated to be 0.12±0.01 t h^{-1} for CH_4 and 110±18 t h^{-1} for CO_2. The uncertainties for the estimates were derived from detailed analyses of each uncertainty source including measurement error in mixing ratio and wind speed, the near-surface wind extrapolation, the near-surface mixing ratio extrapolation, box-top mixing ratio, box-top height and deconvolution. For cases that uses the Air Sampler system instead of online measuring instruments, as the CO_2 and CH_4 time series measured from the Air Sampler were deconvoluted to restore the unsmoothed time series before putting into the TREEA algorithm, it is necessary to account for the uncertainty that comes from deconvolution. Time series before and after deconvolution were applied to the TERRA algorithm to obtain the total emission rates, calculation shows that emission rates before and after deconvolution vary within 1%.

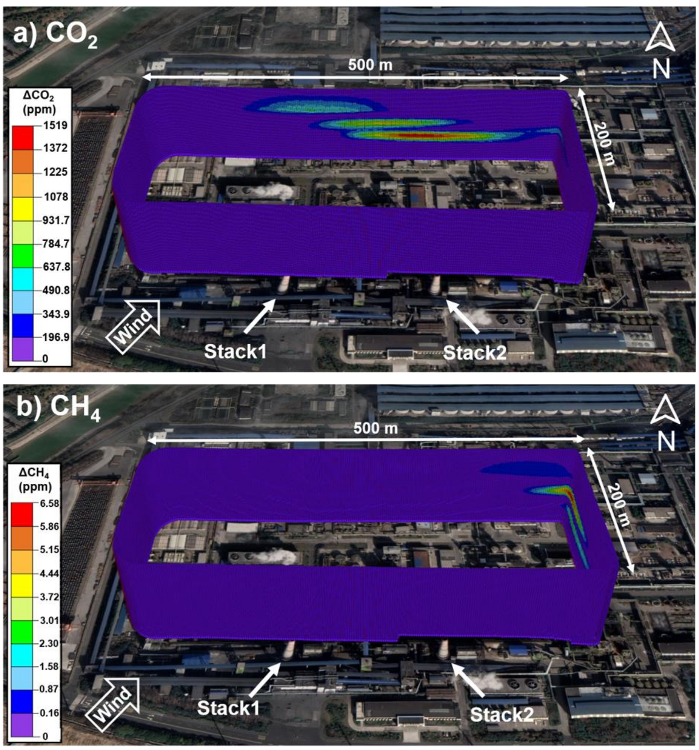

Figure 5. Virtual flight box for monitoring CO_2 (a) and CH_4 (b) during the flight. The CO_2 and CH_4 plumes were captured on the north and east wall respectively. The wind came from the southwestern direction. Sattilite imagery © Google Earth 2019

6.4 Comparison with Gaussian Inversion Approach

The TERRA computation results can be further evaluated. Of the multiple CH_4 plumes that were captured on the north and east walls of the virtual box, the largest CH_4 one resembles a nearly perfect Gaussian plume distribution and is clearly associated with the east stack of the two, for which the emission rate may be recalculated using the Gaussian plume model. The Gaussian plume model makes basic assumptions that the plume is emitted from a point source and that the atmospheric turbulence is constant in space and time(Visscher, 2014). In this study, the captured plume was completely elevated and thus not constrained by boundaries. In the absence of boundaries, the equation for pollutant mixing ratios in Gaussian plumes is as follows:

$$c = \frac{Q}{2\pi \bar{u} \sigma_y \sigma_z} exp\left(-\frac{y^2}{2\sigma_y^2}\right) exp\left(-\frac{(z-h)^2}{2\sigma_z^2}\right) \quad (12)$$

where c is the concentration at a given position x, y and z (g m^{-3}), Q is the emission rate (g s^{-1}), $\bar{u}$ is the mean wind speed (m s^{-1}), h is the effective source height (m) and σ_y and σ_z are dispersion parameters in the horizontal (lateral) and vertical directions respectively (m).

The dispersion parameters σ_y and σ_z were obtained by fitting the spatial distribution of CH_4 mixing ratios into a Gaussian function. As the wall intercepting the plume is not perpendicular to the wind direction, the plume was projected to a different virtual wall perpendicular to the wind direction before fitting the Gaussian function. For the separate CH_4 plume, the Gaussian plume model gives an emission rate of 49 ± 24 kg h^{-1}. The uncertainty is quantified by considering the accuracy of mixing ratio measurement, the variation of wind speed and the confidence interval for the dispersion parameters given by Gaussian function fitting. The TERRA algorithm is able to obtain the emission rate for a selected section through a certain area of the screen. For this isolated CH_4 plume, the TERRA algorithm computed an emission rate of 65±8 kg h^{-1}. The number is comparable to the emission rate estimation from the Gaussian plume model, showing the reliability of top-down emission estimation approaches of both TERRA and the Gaussian plume model analyses of the UAV measurements.

6.5 Validation of UAV-based Emissions and Comparison with IPCC-based Emissions

Coking process is one of the highest energy-consuming operations during iron and steel production that tends to emit large amounts of CO_2 and CH_4. According to the Chinese national GHG inventory report, CO_2 and CH_4 emissions from coke production in iron and steel production processes were calculated using the Tier 1 method in the IPCC Guidelines(Ministry of Ecology and Environment of of China, 2018). In the Tier 1 method, default emission factors for coke production are used to estimate the CO_2 and CH_4 emissions without considering local variations, respectively,

$$E_{CO_2} = P_{coke} \times EF_{CO_2} \ and \ E_{CH_4} = P_{coke} \times EF_{CH_4} \tag{13}$$

where E_{CO_2} and E_{CH_4} represents the CO_2 and CH_4 emission rates from coke production, P_{coke} represents coke production, EF_{CO_2} and EF_{CH_4} are the IPCC default emission factors for CO_2 and CH_4, which are 0.56 t CO_2/t of coke and 0.1 g CH_4/t of coke, respectively. The measured Shagang coking plant consists of two coke oven batteries, each with its own stack. Each battery produced 127.8 t coke h^{-1}, thus totalling 255.6 t coke h^{-1} (P_{coke}) between the two batteries during the UAV measurement period with a coke yield of 78.5%. A material balance analysis revealed that CO_2 emitted from the stacks during the full coking process was 103±32 t CO_2 h^{-1} (SI Section S3). In comparison, the UAV measurement-based emission rate obtained in this study is 110±18 t CO_2 h^{-1}, which is consistent with the CO_2 emissions based on the material balance analysis. For comparison, multiplying the IPCC default emission factor with the coke production at the Shagang coking plant yields an emission rate from coking of 143 t CO_2 h^{-1}, higher than either the material balance based result by about 39% or the UAV-based result by 30%. This suggests that the IPCC default emission factor is too high for this particular coking plant.

On the other hand, the UAV-measurement based emission of 0.12±0.014 t h^{-1} for CH_4 is four orders of magnitude higher than 1.28×10^{-5} t h^{-1} emissions for CH_4 estimated using the IPCC Tier 1 emission factor EF_{CH_4}. The IPCC emission factor for coke production is derived by averaging plant-specific CH_4 emissions data for 11 European coke plants reported in the IPPC I&S BAT Document(European IPPC Bureau, 2001), but information about the data collection method such as sampling methods, analysis methods, time intervals, computation methods and reference conditions is not available according the report. While the present UAV measurement represent a one-time measurement and it is difficult to determine the representativeness of this emission rate, the fact of the large discrepancies suggests that real world emission factors can be significantly different from the default emission factors. The additional CH_4 may come from taps leakage or door leakage in addition to the conventional combustion process during coke production. Both reasons point to a need for further emission measurements to determine the local emission factors and a further validation of the CH_4 emission factors of coke production.

7 Conclusions

In this paper, we present the development of a UAV measurement system for quantifying GHG emissions at facility levels. The key element of this system is a newly designed air sampler, consisting of a 150-meter-long thin-walled stainless steel tube with remote-controlled time stamping. Through laboratory testing, we found that the air sampler generated smoothed time series data compared to online measurement by the CRDS analyzer. To addressing the smoothing effect, we

Atmospheric Measurement Techniques Discussions
Open Access

developed a deconvolution algorithm to restore the resolution of the time series obtained by the air sampler. For field validation, the new UAV measurement system was deployed at the Shagang Steel to obtain CO_2 and CH_4 emissions from the main coking plant at Shagang Steel. Mole fractions of CO_2 and CH_4 together with meteorological parameters were measured during the test flight. The mass-balance algorithm TERRA was used to estimate the coking plant CO_2 and CH_4 emission rates based on the UAV-measured data. For further analysis, we compared these emission results with those derived using Gaussian plume inversion approach and carbon material balance methods, demonstrating good consistency among different approaches. In addition, when compared the top-down UAV-based measurement results to that derived from the bottom-up emission inventory method, the present findings indicated that the use of IPCC emission factors for emission calculations can lead to overestimation.

Acknowledgment. This project was supported by a grant from the National Natural Science Foundation of China Creative Research Group Fund (22221004).

Data availability. Data are available upon request by the corresponding author.

Author contribution. TH, CX, YL and, SML conducted the fieldwork with the support by XG, XZ, and FB. TH and CX conducted laboratory experiments with the guidance by SML. TH performed the primary data analysis, and wrote the initial draft of the manuscript. YH provided expertise in model analysis. Algorithm programming was provided by YL. YY and YZ did the wind data correction. SML reviewd and edited the manuscript, and ensured the accuracy and integrity of the study.

Competing interests. The authors declare that they have no conflictof interest.

Reference

Allen, G., Hollingsworth, P., Kabbabe, K., Pitt, J. R., Mead, M. I., Illingworth, S., Roberts, G., Bourn, M., Shallcross, D. E., and Percival, C. J.: The development and trial of an unmanned aerial system for the measurement of methane flux from landfill and greenhouse gas emission hotspots, Waste Manag, 87, 883-892, 10.1016/j.wasman.2017.12.024, 2019.

Andersen, T., Scheeren, B., Peters, W., and Chen, H.: A UAV-based active AirCore system for measurements of greenhouse gases, Atmospheric Measurement Techniques, 11, 2683-2699, 10.5194/amt-11-2683-2018, 2018.

Andersen, T., Vinkovic, K., de Vries, M., Kers, B., Necki, J., Swolkien, J., Roiger, A., Peters, W., and Chen, H.: Quantifying methane emissions from coal mining ventilation shafts using an unmanned aerial vehicle (UAV)-based active AirCore system, Atmospheric Environment: X, 12, 10.1016/j.aeaoa.2021.100135, 2021.

Arias, P. A., N. Bellouin, E. Coppola, R.G. Jones, G. Krinner, J. Marotzke, V. Naik, M.D. Palmer, G.-K. Plattner, J. Rogelj, M. Rojas, J. Sillmann, T. Storelvmo, P.W. Thorne, B. Trewin, K. Achuta Rao, B. Adhikary, R.P. Allan, K. Armour, G.

Bala, R. Barimalala, S. Berger, J.G. Canadell, C. Cassou, A. Cherchi, W. Collins, W.D. Collins, S.L. Connors, S. Corti, F. Cruz, F.J. Dentener, C. Dereczynski, A. Di Luca, A. Diongue Niang, F.J. Doblas-Reyes, A. Dosio, H. Douville, F. Engelbrecht, V. Eyring, E. Fischer, P. Forster, B. Fox-Kemper, J.S. Fuglestvedt, J.C. Fyfe, N.P. Gillett, L. Goldfarb, I. Gorodetskaya, J.M. Gutierrez, R. Hamdi, E. Hawkins, H.T. Hewitt, P. Hope, A.S. Islam, C. Jones, D.S. Kaufman, R.E. Kopp, Y. Kosaka, J. Kossin, S. Krakovska, J.-Y. Lee, J. Li, T. Mauritsen, T.K. Maycock, M. Meinshausen, S.-K. Min, P.M.S. Monteiro, T. Ngo-Duc, F. Otto, I. Pinto, A. Pirani, K. Raghavan, R. Ranasinghe, A.C. Ruane, L. Ruiz, J.-B. Sallée, B.H. Samset, S. Sathyendranath, S.I. Seneviratne, A.A. Sörensson, S. Szopa, I. Takayabu, A.-M. Tréguier, B. van den Hurk, R. Vautard, K. von Schuckmann, S. Zaehle, X. Zhang, and K. Zickfeld: Technical Summary. In Climate Change 2021: The Physical Science Basis. Contribution of Working Group I to the Sixth Assessment Report of the Intergovernmental Panel on Climate Change [Masson-Delmotte, V., P. Zhai, A. Pirani, S.L. Connors, C. Péan, S. Berger, N. Caud, Y. Chen, L. Goldfarb, M.I. Gomis, M. Huang, K. Leitzell, E. Lonnoy, J.B.R. Matthews, T.K. Maycock, T. Waterfield, O. Yelekçi, R. Yu, and B. Zhou (eds.)], Cambridge University Press, Cambridge, United Kingdom and New York, NY, USA, 33-144, 2021.

Baray, S., Darlington, A., Gordon, M., Hayden, K. L., Leithead, A., Li, S.-M., Liu, P. S. K., Mittermeier, R. L., Moussa, S. G., O'Brien, J., Staebler, R., Wolde, M., Worthy, D., and McLaren, R.: Quantification of methane sources in the Athabasca Oil Sands Region of Alberta by aircraft mass balance, Atmospheric Chemistry and Physics, 18, 7361-7378, 10.5194/acp-18-7361-2018, 2018.

Bel Hadj Ali, N., Abichou, T., and Green, R.: Comparing estimates of fugitive landfill methane emissions using inverse plume modeling obtained with Surface Emission Monitoring (SEM), Drone Emission Monitoring (DEM), and Downwind Plume Emission Monitoring (DWPEM), J Air Waste Manag Assoc, 70, 410-424, 10.1080/10962247.2020.1728423, 2020.

Brantley, H. L., Thoma, E. D., Squier, W. C., Guven, B. B., and Lyon, D.: Assessment of methane emissions from oil and gas production pads using mobile measurements, Environ Sci Technol, 48, 14508-14515, 10.1021/es503070q, 2014.

Brownlow, R., Lowry, D., Thomas, R. M., Fisher, R. E., France, J. L., Cain, M., Richardson, T. S., Greatwood, C., Freer, J., Pyle, J. A., MacKenzie, A. R., and Nisbet, E. G.: Methane mole fraction and δ13C above and below the trade wind inversion at Ascension Island in air sampled by aerial robotics, Geophysical Research Letters, 43, 10.1002/2016gl071155, 2016.

Canadell, J. G., P.M.S. Monteiro, M.H. Costa, L. Cotrim da Cunha, P.M. Cox, A.V. Eliseev, S. Henson, M. Ishii, S. Jaccard, C. Koven, A. Lohila, P.K. Patra, S. Piao, J. Rogelj, S. Syampungani, S. Zaehle, and K. Zickfeld: Global Carbon and other Biogeochemical Cycles and Feedbacks. In Climate Change 2021: The Physical Science Basis. Contribution of Working Group I to the Sixth Assessment Report of the Intergovernmental Panel on Climate Change [Masson-Delmotte, V., P. Zhai,

A. Pirani, S.L. Connors, C. Péan, S. Berger, N. Caud, Y. Chen, L. Goldfarb, M.I. Gomis, M. Huang, K. Leitzell, E. Lonnoy, J.B.R. Matthews, T.K. Maycock, T. Waterfield, O. Yelekçi, R. Yu, and B. Zhou (eds.)], Cambridge University Press, Cambridge, United Kingdom and New York, NY, USA, 673-816, 2021.

Chang, C. C., Wang, J. L., Chang, C. Y., Liang, M. C., and Lin, M. R.: Development of a multicopter-carried whole air sampling apparatus and its applications in environmental studies, Chemosphere, 144, 484-492, 10.1016/j.chemosphere.2015.08.028, 2016.

Cheng, Y., Li, S. M., Liggio, J., Gordon, M., Darlington, A., Zheng, Q., Moran, M., Liu, P., and Wolde, M.: Top-Down Determination of Black Carbon Emissions from Oil Sand Facilities in Alberta, Canada Using Aircraft Measurements, Environ Sci Technol, 54, 412-418, 10.1021/acs.est.9b05522, 2020.

De Boisblanc, I., Dodbele, N., Kussmann, L., Mukherji, R., Chestnut, D., Phelps, S., Lewin, G. C., and de Wekker, S.: Designing a hexacopter for the collection of atmospheric flow data, 2014 Systems and Information Engineering Design Symposium (SIEDS), 147-152, 10.1109/SIEDS.2014.6829915,

Etminan, M., Myhre, G., Highwood, E., and Shine, K.: Radiative forcing of carbon dioxide, methane, and nitrous oxide: A significant revision of the methane radiative forcing, Geophysical Research Letters, 43, 12,614-612,623, 10.1002/2016GL071930, 2016.

Galfalk, M., Nilsson Paledal, S., and Bastviken, D.: Sensitive Drone Mapping of Methane Emissions without the Need for Supplementary Ground-Based Measurements, ACS Earth Space Chem, 5, 2668-2676, 10.1021/acsearthspacechem.1c00106, 2021.

Golston, L., Aubut, N., Frish, M., Yang, S., Talbot, R., Gretencord, C., McSpiritt, J., and Zondlo, M.: Natural Gas Fugitive Leak Detection Using an Unmanned Aerial Vehicle: Localization and Quantification of Emission Rate, Atmosphere, 9, 10.3390/atmos9090333, 2018.

Gordon, M., Li, S. M., Staebler, R., Darlington, A., Hayden, K., O'Brien, J., and Wolde, M.: Determining air pollutant emission rates based on mass balance using airborne measurement data over the Alberta oil sands operations, Atmospheric Measurement Techniques, 8, 3745-3765, 10.5194/amt-8-3745-2015, 2015.

Gulev, S. K., P.W. Thorne, J. Ahn, F.J. Dentener, C.M. Domingues, S. Gerland, D. Gong, D.S. Kaufman, H.C. Nnamchi, J. Quaas, J.A. Rivera, S. Sathyendranath, S.L. Smith, B. Trewin, K. von Schuckmann, and R.S. Vose: Changing State of the Climate System. In Climate Change 2021: The Physical Science Basis. Contribution of Working Group I to the Sixth Assessment Report of the Intergovernmental Panel on Climate Change [Masson-Delmotte, V., P. Zhai, A. Pirani, S.L. Connors, C. Péan, S. Berger, N. Caud, Y. Chen, L. Goldfarb, M.I. Gomis, M. Huang, K. Leitzell, E. Lonnoy, J.B.R. Matthews, T.K. Maycock, T. Waterfield, O. Yelekçi, R. Yu, and B. Zhou (eds.)], Cambridge University Press, Cambridge,

https://doi.org/10.5194/amt-2023-113
Preprint. Discussion started: 24 July 2023

Atmospheric Measurement Techniques Discussions

United Kingdom and New York, NY, USA, 287-422, 2021.

Hasanbeigi, A.: Steel Climate Impact - An International Benchmarking of Energy and CO2 Intensities, Global Efficiency Intelligence, Florida, United States, 2022.

Hayden, K., Li, S.-M., Makar, P., Liggio, J., Moussa, S. G., Akingunola, A., McLaren, R., Staebler, R. M., Darlington, A., O'Brien, J., Zhang, J., Wolde, M., and Zhang, L.: New methodology shows short atmospheric lifetimes of oxidized sulfur and nitrogen due to dry deposition, Atmospheric Chemistry and Physics, 21, 8377-8392, 10.5194/acp-21-8377-2021, 2021.

Helfter, C., Tremper, A. H., Halios, C. H., Kotthaus, S., Bjorkegren, A., Grimmond, C. S. B., Barlow, J. F., and Nemitz, E.: Spatial and temporal variability of urban fluxes of methane, carbon monoxide and carbon dioxide above London, UK, Atmospheric Chemistry and Physics, 16, 10543-10557, 10.5194/acp-16-10543-2016, 2016.

Karion, A., Sweeney, C., Tans, P., and Newberger, T.: AirCore: An innovative atmospheric sampling system, Journal of Atmospheric and Oceanic Technology, 27, 1839-1853, 10.1175/2010JTECHA1448.1, 2010.

Li, H. Z., Mundia-Howe, M., Reeder, M. D., and Pekney, N. J.: Gathering Pipeline Methane Emissions in Utica Shale Using an Unmanned Aerial Vehicle and Ground-Based Mobile Sampling, Atmosphere, 11, 10.3390/atmos11070716, 2020.

Li, S. M., Leithead, A., Moussa, S. G., Liggio, J., Moran, M. D., Wang, D., Hayden, K., Darlington, A., Gordon, M., Staebler, R., Makar, P. A., Stroud, C. A., McLaren, R., Liu, P. S. K., O'Brien, J., Mittermeier, R. L., Zhang, J., Marson, G., Cober, S. G., Wolde, M., and Wentzell, J. J. B.: Differences between measured and reported volatile organic compound emissions from oil sands facilities in Alberta, Canada, Proc Natl Acad Sci U S A, 114, E3756-E3765, 10.1073/pnas.1617862114, 2017.

Liggio, J., Li, S. M., Staebler, R. M., Hayden, K., Darlington, A., Mittermeier, R. L., O'Brien, J., McLaren, R., Wolde, M., Worthy, D., and Vogel, F.: Measured Canadian oil sands CO2 emissions are higher than estimates made using internationally recommended methods, Nat Commun, 10, 1863, 10.1038/s41467-019-09714-9, 2019.

Liggio, J., Li, S. M., Hayden, K., Taha, Y. M., Stroud, C., Darlington, A., Drollette, B. D., Gordon, M., Lee, P., Liu, P., Leithead, A., Moussa, S. G., Wang, D., O'Brien, J., Mittermeier, R. L., Brook, J. R., Lu, G., Staebler, R. M., Han, Y., Tokarek, T. W., Osthoff, H. D., Makar, P. A., Zhang, J., Plata, D. L., and Gentner, D. R.: Oil sands operations as a large source of secondary organic aerosols, Nature, 534, 91-94, 10.1038/nature17646, 2016.

Lin, F. and Jin, C.: An improved Wiener deconvolution filter for high-resolution electron microscopy images, Micron, 50, 1-6, 10.1016/j.micron.2013.03.005, 2013.

Miller, S. M., Wofsy, S. C., Michalak, A. M., Kort, E. A., Andrews, A. E., Biraud, S. C., Dlugokencky, E. J., Eluszkiewicz, J., Fischer, M. L., Janssens-Maenhout, G., Miller, B. R., Miller, J. B., Montzka, S. A., Nehrkorn, T., and Sweeney, C.:

https://doi.org/10.5194/amt-2023-113
Preprint. Discussion started: 24 July 2023

Atmospheric Measurement Techniques Discussions

Anthropogenic emissions of methane in the United States, Proc Natl Acad Sci U S A, 110, 20018-20022, 10.1073/pnas.1314392110, 2013.

Morales, R., Ravelid, J., Vinkovic, K., Korbeń, P., Tuzson, B., Emmenegger, L., Chen, H., Schmidt, M., Humbel, S., and Brunner, D.: Controlled-release experiment to investigate uncertainties in UAV-based emission quantification for methane point sources, Atmospheric Measurement Techniques, 15, 2177-2198, 10.5194/amt-15-2177-2022, 2022.

Nathan, B. J., Golston, L. M., O'Brien, A. S., Ross, K., Harrison, W. A., Tao, L., Lary, D. J., Johnson, D. R., Covington, A. N., Clark, N. N., and Zondlo, M. A.: Near-Field Characterization of Methane Emission Variability from a Compressor Station Using a Model Aircraft, Environ Sci Technol, 49, 7896-7903, 10.1021/acs.est.5b00705, 2015.

Palomaki, R. T., Rose, N. T., van den Bossche, M., Sherman, T. J., and De Wekker, S. F. J.: Wind Estimation in the Lower Atmosphere Using Multirotor Aircraft, Journal of Atmospheric and Oceanic Technology, 34, 1183-1191, 10.1175/jtech-d-16-0177.1, 2017.

Rella, C. W., Tsai, T. R., Botkin, C. G., Crosson, E. R., and Steele, D.: Measuring emissions from oil and natural gas well pads using the mobile flux plane technique, Environmental science & technology, 49, 4742-4748, 10.1021/acs.est.5b00099, 2015.

Saunois, M., Stavert, A. R., Poulter, B., Bousquet, P., Canadell, J. G., Jackson, R. B., Raymond, P. A., Dlugokencky, E. J., Houweling, S., Patra, P. K., Ciais, P., Arora, V. K., Bastviken, D., Bergamaschi, P., Blake, D. R., Brailsford, G., Bruhwiler, L., Carlson, K. M., Carrol, M., Castaldi, S., Chandra, N., Crevoisier, C., Crill, P. M., Covey, K., Curry, C. L., Etiope, G., Frankenberg, C., Gedney, N., Hegglin, M. I., Höglund-Isaksson, L., Hugelius, G., Ishizawa, M., Ito, A., Janssens-Maenhout, G., Jensen, K. M., Joos, F., Kleinen, T., Krummel, P. B., Langenfelds, R. L., Laruelle, G. G., Liu, L., Machida, T., Maksyutov, S., McDonald, K. C., McNorton, J., Miller, P. A., Melton, J. R., Morino, I., Müller, J., Murguia-Flores, F., Naik, V., Niwa, Y., Noce, S., O'Doherty, S., Parker, R. J., Peng, C., Peng, S., Peters, G. P., Prigent, C., Prinn, R., Ramonet, M., Regnier, P., Riley, W. J., Rosentreter, J. A., Segers, A., Simpson, I. J., Shi, H., Smith, S. J., Steele, L. P., Thornton, B. F., Tian, H., Tohjima, Y., Tubiello, F. N., Tsuruta, A., Viovy, N., Voulgarakis, A., Weber, T. S., van Weele, M., van der Werf, G. R., Weiss, R. F., Worthy, D., Wunch, D., Yin, Y., Yoshida, Y., Zhang, W., Zhang, Z., Zhao, Y., Zheng, B., Zhu, Q., Zhu, Q., and Zhuang, Q.: The Global Methane Budget 2000–2017, Earth System Science Data, 12, 1561-1623, 10.5194/essd-12-1561-2020, 2020.

Shah, A., Ricketts, H., Pitt, J. R., Shaw, J. T., Kabbabe, K., Leen, J. B., and Allen, G.: Unmanned aerial vehicle observations of cold venting from exploratory hydraulic fracturing in the United Kingdom, Environmental Research Communications, 2, 021003, 10.1088/2515-7620/ab716d, 2020.

Shaw, J. T., Shah, A., Yong, H., and Allen, G.: Methods for quantifying methane emissions using unmanned aerial vehicles:

https://doi.org/10.5194/amt-2023-113
Preprint. Discussion started: 24 July 2023

a review, Philos Trans A Math Phys Eng Sci, 379, 20200450, 10.1098/rsta.2020.0450, 2021.

Takano, T. and Ueyama, M.: Spatial variations in daytime methane and carbon dioxide emissions in two urban landscapes, Sakai, Japan, Urban Climate, 36, 100798, 10.1016/j.uclim.2021.100798, 2021.

Turner, A. J., Frankenberg, C., and Kort, E. A.: Interpreting contemporary trends in atmospheric methane, Proc Natl Acad Sci U S A, 116, 2805-2813, 10.1073/pnas.1814297116, 2019.

Turner, A. J., Jacob, D. J., Wecht, K. J., Maasakkers, J. D., Lundgren, E., Andrews, A. E., Biraud, S. C., Boesch, H., Bowman, K. W., Deutscher, N. M., Dubey, M. K., Griffith, D. W. T., Hase, F., Kuze, A., Notholt, J., Ohyama, H., Parker, R., Payne, V. H., Sussmann, R., Sweeney, C., Velazco, V. A., Warneke, T., Wennberg, P. O., and Wunch, D.: Estimating global and North American methane emissions with high spatial resolution using GOSAT satellite data, Atmospheric Chemistry and Physics, 15, 7049-7069, 10.5194/acp-15-7049-2015, 2015.

Tuzson, B., Morales, R., Graf, M., Scheidegger, P., Looser, H., Kupferschmid, A., and Emmenegger, L.: Bird's-eye View of Localized Methane Emission Sources: Highlights of Analytical Sciences in Switzerland, Chimia, 75, 802-802, 10.2533/chimia.2021.802, 2021.

Vinkovic, K., Andersen, T., de Vries, M., Kers, B., van Heuven, S., Peters, W., Hensen, A., van den Bulk, P., and Chen, H.: Evaluating the use of an Unmanned Aerial Vehicle (UAV)-based active AirCore system to quantify methane emissions from dairy cows, Sci Total Environ, 831, 154898, 10.1016/j.scitotenv.2022.154898, 2022.

Visscher, A. D.: Air Dispersion Modeling: Foundations and Applications, John Wiley & Sons, Inc., Hoboken, New Jersey2014.

Wolf, C. A., Hardis, R. P., Woodrum, S. D., Galan, R. S., Wichelt, H. S., Metzger, M. C., Bezzo, N., Lewin, G. C., and de Wekker, S. F.: Wind data collection techniques on a multi-rotor platform, 2017 Systems and Information Engineering Design Symposium (SIEDS), 32-37, 10.1109/SIEDS.2017.7937739,

Yang, Y.: A UAV based 3-D wind measurement methodology for applications to air pollutant emission quantification, in preparation for submission to Environmental Science and Technology, 2023.

Zhou, S., Peng, S., Wang, M., Shen, A., and Liu, Z.: The Characteristics and Contributing Factors of Air Pollution in Nanjing: A Case Study Based on an Unmanned Aerial Vehicle Experiment and Multiple Datasets, Atmosphere, 9, 10.3390/atmos9090343, 2018.